

# Submillimetre and far-infrared spectral energy distributions of galaxies: the luminosity–temperature relation and consequences for photometric redshifts

A. W. Blain,<sup>1</sup> V. E. Barnard,<sup>2</sup> and S. C. Chapman<sup>1</sup>

<sup>1</sup> *California Institute of Technology, 105-24, Pasadena, CA 91125, USA*

<sup>2</sup> *Cavendish Astrophysics, Madingley Road, Cambridge, CB3 0HE*

4 October 2018

## ABSTRACT

The spectral energy distributions (SEDs) of dusty high-redshift galaxies are poorly sampled in frequency and spatially unresolved. Their form is crucially important for estimating the large luminosities of these galaxies accurately, for providing circumstantial evidence concerning their power sources, and for estimating their redshifts in the absence of spectroscopic information. We discuss the suite of parameters necessary to describe their SEDs adequately without introducing unnecessary complexity. We compare directly four popular descriptions, explain the key degeneracies between the parameters in each when confronted with data, and highlight the differences in their best-fitting values. Using one representative SED model, we show that fitting to even a large number of radio, submillimetre and far-infrared (far-IR) continuum colours provides almost no power to discriminate between the redshift and dust temperature of an observed galaxy, unless an accurate relationship with a tight scatter exists between luminosity and temperature for the whole galaxy population. We review our knowledge of this luminosity–dust temperature relation derived from three galaxy samples, to better understand the size of these uncertainties. Contrary to recent claims, we stress that far-IR-based photometric redshifts are unlikely to be sufficiently accurate to impose useful constraints on models of galaxy evolution: finding spectroscopic redshifts for distant dusty galaxies will remain essential.

**Key words:** radiation mechanisms: thermal – dust, extinction – galaxies: general – galaxies: photometry – infrared: galaxies – submillimetre

## 1 INTRODUCTION

The rest-frame far-infrared (far-IR) thermal emission from dust grains heated by various sources – the diffuse interstellar radiation field (ISRF) in galaxies, sites of active star formation, and a central active galactic nucleus (AGN) – can dominate the spectral energy distribution (SED) of galaxies (Soifer & Neugebauer 1991; Sanders & Mirabel 1996). The most luminous galaxy apparent in the Universe (APM08279+5255; Irwin et al. 1998) emits approximately 60 per cent of its bolometric luminosity in the far-IR waveband, while low-redshift galaxies with blue optical colours that were detected by the *IRAS* satellite also release about 60 per cent of their total bolometric luminosity as thermal radiation from dust (Mazzarella & Balzano 1986). Even the most quiescent spiral galaxies such as the Milky Way emit of order 30 per cent of their total luminosity from dust (Reach et al. 1995; Alton et al. 1998; Dale et al. 2001; Dale & Helou 2002). Dust emission remains important at high redshifts.

The most distant quasi-stellar objects (QSOs) (Benford et al. 1999; Carilli et al. 2001; Isaak et al. 2002) and more typical, but still very luminous galaxies detected in submillimetre(submm) wave surveys (Blain et al. 2002; Smail et al. 2002) emit strongly at rest-frame far-IR wavelengths.

As compared with the rich variety of features in the SEDs of galaxies at near-IR, optical and ultraviolet wavelengths, the far-IR SED is simple, dominated by a smooth pseudo-thermal continuum emission spectrum. At most about 1 per cent of the emitted energy is associated with spectral lines from atomic fine-structure and molecular rotational transitions (Malhotra et al. 1997; Luhman et al. 1998; Combes, Maoli & Omont 1999; Blain et al. 2000). The mid-IR spectra of galaxies from 10 to 30  $\mu\text{m}$  are expected to be significantly more complex, especially because of broad line emission from polycyclic aromatic hydrocarbon (PAH) molecules (Dale et al. 2001).

A variety of models have been used to describe the

far-IR SEDs of dusty galaxies. We compare four well-constrained descriptions with data for a variety of types of galaxy, and highlight the importance both of degeneracies between the parameters and the need to avoid baroque descriptions that require a greater number of parameters than can be justified and fixed by existing data. Using one uniform, self-consistent description of the SED we discuss the accuracy of photometric redshifts that can be derived for high-redshift galaxies based on their observed colours, making assumptions concerning their SEDs. We describe in detail the degeneracy between redshift and dust temperature when fitting photometric data for high-redshift galaxies (Blain 1999b; Blain et al. 2002), and discuss the prospects for breaking this degeneracy using information about absolute luminosity, obtained from a luminosity–temperature ( $LT$ ) relation for dusty galaxies. A narrow range of SEDs was included implicitly in recent discussions of the prospects for determining mm-wave photometric redshifts (Hughes et al. 2002; Aretxaga et al. 2003; Dunlop et al. 2003), which leads to encouraging results. We discuss existing data on the  $LT$  relation (Dunne et al. 2000; Stanford et al. 2000; Dale et al. 2001; Dale & Helou 2002; Garrett 2002; Barnard & Blain 2003; Chapman et al. 2003), which leads to a much less optimistic outlook for far-IR/submm photometric redshifts. The observed dispersion in the  $LT$  relation is the key quantity that limits the effectiveness of the technique.

In Section 2 we describe four SED models, and compare them with a range of observed galaxy SEDs. We highlight the consequences of errors in the fitted SEDs and the  $LT$  relation for determining photometric redshifts in Section 3. Finally, in Section 4, we describe the requirements for spectroscopic observations that will remove this uncertainty, and describe the opportunities that much more detailed far-IR SEDs measured using *SIRTF*<sup>1</sup> from 2003 will provide for better understanding the  $LT$  relation and for determining far-IR-based photometric redshifts.

## 2 SED DESCRIPTIONS

Various functions have been used to describe the quasi-blackbody far-IR/submm of the SEDs of dusty galaxies. The parameters that define the SED generally disguise the inevitably complex geometrical mix of dust grains at different temperatures in the interstellar medium of these galaxies, which are often disturbed and interacting, and sometimes very luminous. The far-IR emission is visible at different optical depths in both emitted and scattered radiation.

### 2.1 Single-temperature models

The simplest SED description is based on a blackbody spectrum  $B_\nu \propto \nu^3 / [\exp(h\nu/kT) - 1]$  at a single temperature  $T$ , as a function of frequency  $\nu$ , modified by a frequency-dependent emissivity function  $\epsilon_\nu \propto \nu^\beta$ , where  $\beta$  is in the range 1–2 (Hildebrand 1983). This yields an SED function is

$$f_\nu = \epsilon_\nu B_\nu \propto \nu^{3+\beta} / [\exp(h\nu/kT) - 1]. \quad (1)$$

Note that this function has an exponential Wien dependence when  $\nu \gg kT/h$ . It is necessary to modify this to a shallower form in order to agree with observed SEDs (see Fig. 1). A straightforward way to counteract the mid-IR Wien tail is to substitute a power-law SED,  $f_\nu \propto \nu^{-\alpha}$  at high frequencies, matching the power-law and thermal function (equation 1) with a smooth gradient at a frequency  $\nu'$ , which requires the condition  $d \ln f_\nu(\nu') / d \ln \nu' = -\alpha$  to be satisfied. Three parameters are required to describe the SED:  $T$ ,  $\beta$  and  $\alpha$ . The dust temperature  $T$  determines the frequency of the SED peak, the emissivity index  $\beta$  fixes the power-law index of the SED in the Rayleigh–Jeans regime, and  $\alpha$  sets the slope of the mid-IR SED. This SED was used in the context of studying submm-wave galaxy evolution by Blain et al. (1999a), and has been used without the Wien correction to fit low-redshift SEDs by Dunne et al. (2000).

An alternative ‘optically thick’ functional form substitutes a more complex emissivity function,  $\epsilon_\nu \propto [1 - \exp(\nu/\nu_0)]^\beta$ , to describe the expected increase in the optical depth of dust emission at higher frequencies, leading to an SED function,

$$f_\nu = \epsilon_\nu B_\nu \propto [1 - \exp(\nu/\nu_0)]^\beta B_\nu. \quad (2)$$

This SED has been used by several authors, especially those dealing with the SEDs of galaxies and AGN at the highest redshifts (e.g. Benford et al. 1999; Isaak et al. 2002) where the SED is probed close to its rest-frame peak. This SED is identical to the  $T$ – $\alpha$ – $\beta$  form at long wavelengths, but tends to a pure blackbody at frequencies greater than  $\nu_0$ , as expected from an optically thick source. This function also requires a power-law to temper the SED on the Wien tail, using the parameter  $\alpha$ . Four SED parameters are thus required in this model:  $T$ ,  $\alpha$  and  $\beta$  as before, plus  $\nu_0$ . There is a strong degeneracy between the value of  $\nu_0$  and the values of  $T$  and  $\beta$  (see Section 2.4). Hence, a reasonable value of  $\nu_0$  that corresponds to a frequency close to the 60- and 100- $\mu\text{m}$  *IRAS* bands is usually assumed. Including this frequency-dependent opacity allows a more physical description of the SED, but the parameter  $\nu_0$  is difficult to determine unambiguously from available observed data.

### 2.2 Models with multiple dust temperatures

Descriptions of the SED can include more than one dust temperature. Most notably, these include models based on radiative transfer calculations, in which a continuous distribution of sources is assumed in some geometry, and the temperature distribution of the dust as a function of position is calculated self-consistently to build up an SED (Granato, Danese & Franceschini 1996; Devriendt et al. 1999; Efstathiou, Rowan-Robinson & Siebenmorgen 2000). Note, however, that even for nearby galaxies the spatial and spectral resolution available is insufficient to constrain the  $\sim 10$  parameters required to describe this type of model even in the simplest spherical geometry. When the sub-arcsec resolution of the Atacama Large Millimeter Array (ALMA) interferometer and *James Webb (Next Generation) Space Telescope (NGST)* are available at submm and near/mid-IR wavelengths, respectively, then radiative transfer models will have a role to play in interpreting observations. At present, the quality of available data does not justify the incorporation of such complexity.

<sup>1</sup> See <http://sirtf.caltech.edu>

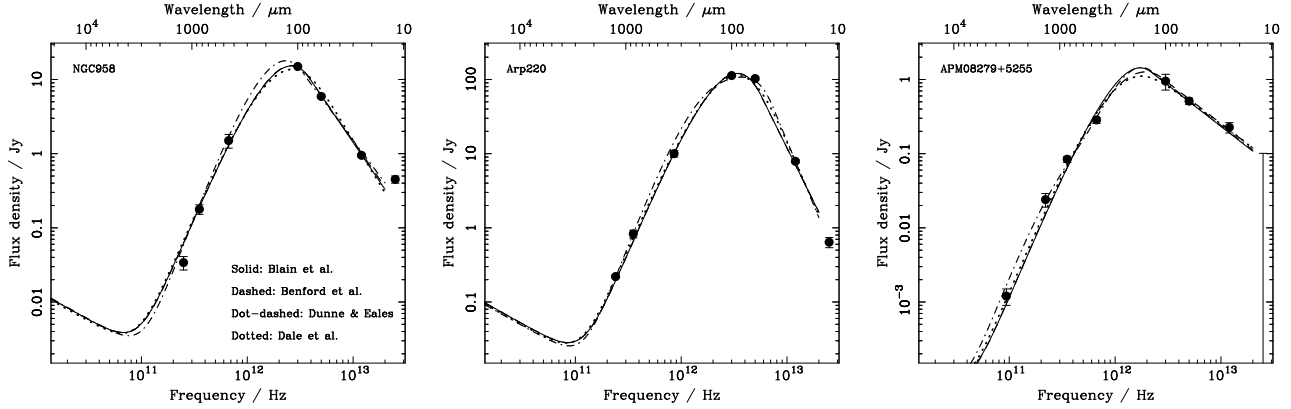


**Figure 1.** The observed SEDs of three well-studied galaxies: the low-redshift ( $z = 0.019$ ) Sb galaxy NGC 958 (Dunne & Eales 2001), the often-quoted prototype low-redshift ( $z = 0.018$ ) ultraluminous dusty galaxy Arp 220, and the galaxy with the greatest apparent luminosity in the Universe APM 08279+5255 (Irwin et al. 1998; Lewis et al. 1998). Four SED models described in Section 2 are compared: a  $T$ - $\alpha$ - $\beta$  model (equation 1), a model with a variable optical depth (equation 2), a model with both a cold and a warm dust component (equation 3) and a model with a power-law dust mass-temperature distribution (equation 4). The parameters required to fit the data in all four models are listed in Table 1: the numerical values differ, but all provide reasonable descriptions of the data, including the radio data for NGC 958 and Arp 220, which is not shown to avoid extending their abscissae over another 2 orders of magnitude. The plotted ranges of frequency are equal, demonstrating the range of different apparent dust temperatures/rest-frame SED peak frequencies and mid-IR spectral indices observed.

**Table 1.** Lists of the best-fitting parameters in the four SED models described in Section 2 (equations 1–4) required to reproduce the observed SEDs of three well-studied galaxies: see Fig. 1. The bolometric luminosities  $L$ , defined as the integral under the SED  $f_\nu$ , normalized to the observed flux density of the galaxy, associated with each model and galaxy are listed. In model 3 a cool component with a dust temperature  $T_c = 20$  K is always added. In model 4 the value of the upper limit to the dust temperature  $T_{\max} = 2000$  K in all cases.

Galaxy	Model 1	Model 2	Model 3	Model 4
NGC 958 $z = 0.019$	$T = 28.8 \pm 1$ K $\alpha = 2.02 \pm 0.2$ $\beta = 1.5^f$ $L = 3.1 \times 10^{11} L_\odot$	$T = 33 \pm 2$ K $\alpha = 2.0 \pm 0.2$ $\beta = 1.5 \pm 0.1$ $\nu_0 = (2.9 \pm 0.5) \times 10^{12}$ Hz $L = 1.8 \times 10^{11} L_\odot$	$T_w = 24.8 \pm 2$ K $\alpha = 1.9 \pm 0.2$ $\beta = 2.0^f$ $F_{wc} = 0.58 \pm 0.2$ $L = 2.6 \times 10^{11} L_\odot$	$T_{\min} = 22.0 \pm 1$ K $\gamma = 7.9 \pm 0.3$ $\beta = 1.5^f$ $L = 2.9 \times 10^{11} L_\odot$
Arp 220 $z = 0.018$	$T = 37.4 \pm 1$ K $\alpha = 2.9 \pm 0.2$ $\beta = 1.5^f$ $L = 1.41 \times 10^{12} L_\odot$	$T = 56 \pm 1.5$ K $\alpha = 3.0 \pm 0.1$ $\beta = 1.55 \pm 0.1$ $\nu_0 = (1.46 \pm 0.1) \times 10^{12}$ Hz $L = 1.43 \times 10^{12} L_\odot$	$T_w = 42.3 \pm 1$ K $\alpha = 3.43 \pm 0.3$ $\beta = 2.0^f$ $F_{wc} = 0.51 \pm 0.1$ $L = 1.47 \times 10^{12} L_\odot$	$T_{\min} = 29.7 \pm 1$ K $\gamma = 8.8 \pm 0.2$ $\beta = 1.5^f$ $L = 1.39 \times 10^{12} L_\odot$
APM 08279+5255 $z = 3.8$	$T = 91 \pm 5$ K $\alpha = 1.1 \pm 0.1$ $\beta = 1.5^f$ $L = 6.7 \times 10^{15} L_\odot$	$T = 187 \pm 10$ K $\alpha = 1.05 \pm 0.15$ $\beta = 1.7 \pm 0.3$ $\nu_0 = (1.4 \pm 0.2) \times 10^{12}$ Hz $L = 3.2 \times 10^{15} L_\odot$	$T_w = 83 \pm 3$ K $\alpha = 1.1^f$ $\beta = 2.0^f$ $F_{wc} = 0.033 \pm 0.01$ $L = 1.0 \times 10^{16} L_\odot$	$T_{\min} = 59.7 \pm 3$ K $\gamma = 6.5 \pm 0.2$ $\beta = 1.5^f$ $L = 3.1 \times 10^{15} L_\odot$

<sup>f</sup> This parameter value was fixed in the fitting process, either to reduce the size of the parameter space being searched or to enforce a physically meaningful value.

Two more practical multi temperature SED descriptions have been used. A two-temperature model by Dunne & Eales (2001) includes a cool component at a fixed temperature of  $T_c = 20$  K to describe dust heated by the general diffuse ISRF of the galaxy, and a component of hotter dust at a temperature  $T_w$ , with a mass fraction  $F_{wc}$ , that is heated more intensely in star-forming regions. Each component is described by a modified blackbody  $\nu^\beta B_\nu$  spectrum, assuming a fixed value of the emissivity index  $\beta = 2$ . The resulting SED function

$$f_\nu \propto \nu^\beta [B_\nu(T_c) + F_{wc} B_\nu(T_w)]. \quad (3)$$

There are 3 free parameters in this model if  $T_c$  is fixed at 20 K and  $\beta$  is fixed at 2.0:  $T_w$  and  $F_{wc}$  to describe the thermal part of the SED, and a power-law index  $\alpha$ , to fix the mid-IR SED. A similar two-temperature model, with a greater spread between the temperatures, is described in the context of the dust emission from galaxies that are members of the Virgo cluster by Popescu et al. (2002).

A fourth, physically motivated, and yet still adequately constrained model was described by Dale et al. (2001), who assumed a power-law distribution of dust masses as a function of temperature, in which the mass of dust heated to a temperature between  $T$  and  $T+dT$ , is given by  $m(T) \propto T^{-\gamma}$ .

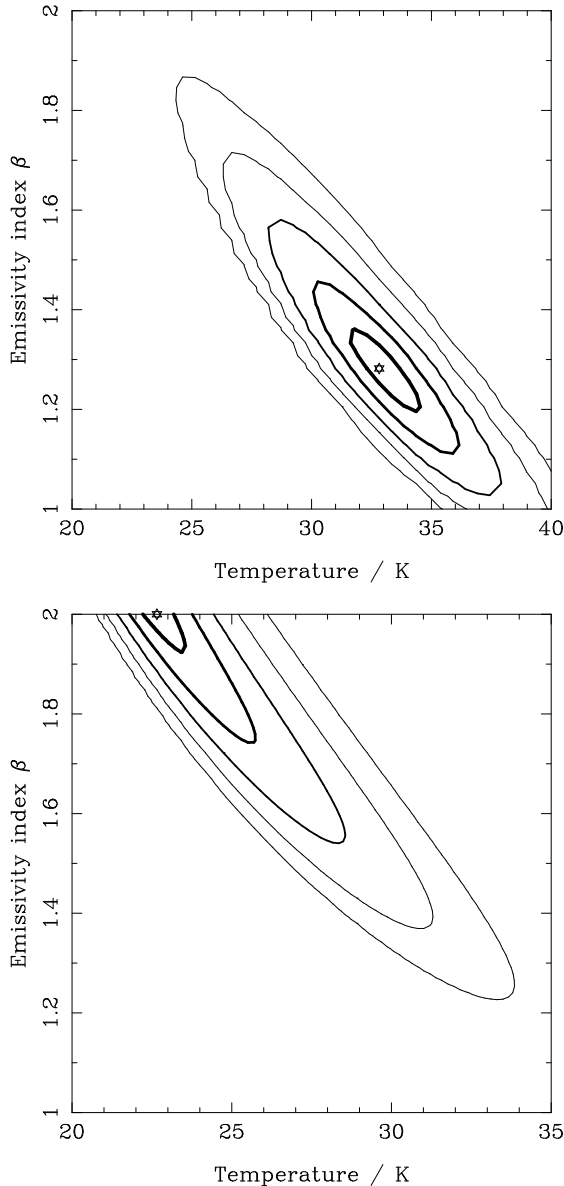


**Figure 2.** Contours of the probability of fitting data for NGC 958, using model 1, as a function of the values of the most important model parameters  $T$  and  $\beta$ . The result for all the data plotted in Fig. 1, plus radio data, is shown in the upper panel, while in the lower panel the results are derived for only the subset of data at 850, 450, 100 and  $60\,\mu\text{m}$  for consistency with Dunne & Eales (2001). The contours are spaced by unit standard deviations away from the best-fitting values, which are marked by a star. A fixed best-fitting value of  $\alpha = 2.02$  is assumed, and  $\beta$  spans the physically plausible range  $1 \rightarrow 2$ . There is a strong degeneracy between  $T$  and  $\beta$  in both panels. Between the two panels the best-fit points remain on a similar  $T$ - $\beta$  trend line, but lie on different tracks. The best-fitting point from the restricted data set prefers the physically implausible  $\beta > 2$  region. Note that if  $\beta$  is fixed at 1.5, then the value of  $T = 28.8\,\text{K}$  listed in Table 1 is the best fitting value in the upper panel.

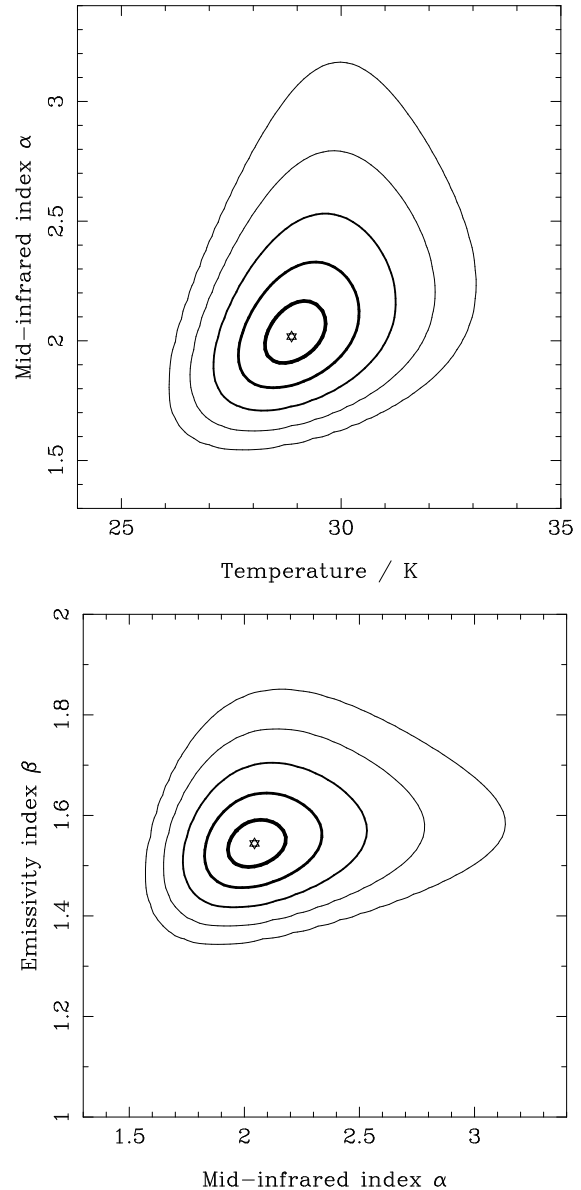


**Figure 3.** The counterpart to Fig. 2 for the two other pairs of parameters:  $T$ - $\alpha$  (upper panel; with  $\beta = 1.5$ ) and  $\alpha$ - $\beta$  (lower panel; with  $T = 29\,\text{K}$ ). In both panels the best-fitting values lie in a well-defined, circular region of the parameter space.

The spectral contribution to the SED from each temperature component is  $\nu^\beta B_\nu$ , and so the composite SED is given by the integral

$$f_\nu \propto \int_{T_{\min}}^{T_{\max}} m(T) \nu^\beta B_\nu dT \propto \int_{T_{\min}}^{T_{\max}} T^{-\gamma} \nu^\beta B_\nu dT. \quad (4)$$

The value of  $\gamma$  effectively determines the mid-IR slope at frequencies  $\nu \gg kT/h$ , and has a close equivalence to  $\alpha$  above. Thus there is no need to introduce another parameter to counteract the Wien tail of the SED here. The value of  $\gamma$  required to produce the same mid-IR spectrum as the other three models is  $\gamma \simeq 4 + \alpha + \beta$  (Blain 1999a). The role of  $T_{\min}$  is equivalent to  $T$  in the other models, and determines the frequency of the peak of the SED, subject to a weak depen-

dence on the value of  $\gamma$ .  $T_{\min}$  must always exceed the cosmic microwave background (CMB) temperature. The value of the maximum temperature  $T_{\max}$  is relatively unimportant, unless  $T_{\min}$  is very high:  $T_{\max}$  was always set to 2000 K to represent the sublimation temperature of the dust. We have thus chosen to keep  $T_{\max}$  fixed and vary both  $T_{\min}$  and  $\gamma$  to fit the data. This model has the minor practical disadvantage that an integral must be performed, or a look-up table employed, to evaluate the SED. In the updated model of Dale & Helou (2002) the value of the emissivity parameter  $\beta$  at wavelengths longward of  $100\ \mu\text{m}$  is now parametrized as a function of the intensity of the ISRF. For simplicity, we adopt a constant value  $\beta = 1.5$  here.

For all four models an additional component of synchrotron radio emission was added, by assuming the conventional far-IR–radio correlation (Condon 1992) between the 1.4-GHz radio emission and the flux densities in the 60- and  $100\text{-}\mu\text{m}$  *IRAS* passbands. This correlation holds with a 0.2-dek dispersion over 4 orders of magnitude in luminosity, and should provide a reasonable representation of the expected radio flux in the absence of additional radio emission from electrons accelerated by an AGN. The details of the extrapolation method are described in Blain (1999a).

### 2.3 Comparison of the SED models with data

The four SED models described above were fitted to data for three well-studied galaxies with very different luminosities and rest-frame SEDs. The results are shown in Fig. 1 and Table 1. The data were obtained from *IRAS* between 12 and  $100\ \mu\text{m}$ , from SCUBA at 450 and  $850\ \mu\text{m}$ , from other ground-based mm-wave telescopes, and from the VLA at 1.4 GHz in the cases of NGC 958 and Arp 220. The SEDs are reasonably well sampled all the way from the mid-IR to the radio waveband. All four models can provide a good description of these SEDs. In models 1 and 4, the emissivity index  $\beta$  was fixed to 1.5 to reduce the size of the parameter space to search in the maximum-likelihood fitting routine, without great loss of generality or hampering the quality of the fit. A key degeneracy between fitted values of  $T$  ( $T_{\min}$  in model 4) and  $\beta$  is described in the next section.

The width of the peak of the model SEDs, defined as the fractional frequency range over which the SED is reduced to half of its peak value, is the feature that differs most significantly from model to model, but never does so by more than a factor of approximately 1.5. The different functional forms of the SED require values of temperature that can have a large dispersion. This is especially true for APM 08279+5255. In model 2 the dust cloud is inferred to become optically thick at frequencies less than the peak of the SED, requiring a much higher temperature to describe the data than in the optically thin models, reflecting the lower effective value of  $\beta$  close to the peak of the SED in the optically-thick model. The peak frequency of the fitted SED is consistent with the data, and the luminosity is within the range spanned by the other three models (see Fig. 1 and Table 1). Hence, model 3 still provides an adequate description of the data. For the other galaxies, the temperature required to fit the data in model 1 is systematically less than that in the optically-thick model 2, again because of the effectively smaller value of  $\beta$  at the SED peak in model 2.

The temperature of the warm component required to fit

SEDs in the two-temperature model 3 depends on the relative intensities of the 25- and  $100\text{-}\mu\text{m}$  *IRAS* flux densities. The value of  $T_{\min}$  required to fit the data in model 4 with a power-law dust mass distribution is always lower than in the other models, reflecting its definition as a lower limit to a distribution of hotter temperatures. The factor by which it is lower than in the other models depends on the value of the mass–temperature function index  $\gamma$  (equation 4): a steeper decline in the proportion of dust at higher temperatures leads to a smaller difference, while a greater fraction of hot dust corresponds to a greater difference.

### 2.4 Degeneracies between fitted SED parameters

The most significant practical degeneracy in fitting the results shown in Fig. 1 in all four models is between the dust temperature  $T$  and the emissivity power-law index  $\beta$ , as illustrated in Fig. 2. This occurs because the peak frequency of the SED scales approximately with the value of  $\beta/T$ , and so the ratio of  $\beta$  and  $T$  must remain approximately constant in order to reproduce the data. In model 4 there is an effective dust temperature  $T$  that reflects the range of temperatures present. For a fixed value of  $\gamma$  this effective temperature is determined by the value of  $T_{\min}$ .

Considering a subset of the data can modify the position of the best fit values significantly along the extended direction of the probability contours in the figure. The other pairs of parameters  $T$ – $\alpha$  and  $\alpha$ – $\beta$  do not show such a degeneracy – the probability contours determined for their fit to the SED data are almost circular (Fig. 3) – and so these pairs of parameters have unique well-determined values when the model provides a good description of the observed SED. Note that the bolometric far-IR luminosity of the galaxy that is derived by integrating the SED in frequency from 100 GHz to the frequency equivalent to a wavelength of  $1\ \mu\text{m}$  changes along the ridge of the probability curve shown in the upper panel of Fig. 2. The inferred luminosity increases smoothly along the ridge from  $2.6 \times 10^{11}\ L_{\odot}$  when  $T = 23\ \text{K}$  to  $4.4 \times 10^{11}\ L_{\odot}$  when  $T = 40\ \text{K}$ , with  $L = 3.1 \times 10^{11}\ L_{\odot}$  at the best-fitting value of 28 K if  $\beta = 1.5$ . Hence, there is little practical difficulty in using this description – neither the luminosity nor the peak frequency of the SED differs significantly as the permitted region in the  $T$ – $\beta$  parameter space is traversed. There is however a real problem in trying to associate the values of the fitted parameters with the true physical properties of the dust grains that generate the emission.

With the exception of  $T$  and  $\beta$  in all models ( $T_{\min}$  and  $\beta$  in model 4) and the pairs  $T$ – $\nu_0$  and  $F_{\text{wc}}$ – $T_{\text{w}}$  in models 2 and 3 respectively, the parameters are well determined. The well-determined pairs of parameters  $T$ – $\alpha$  and  $\alpha$ – $\beta$  are illustrated in Fig. 3, with almost circular probability contours. The probabilities for the relatively ill-constrained pairs discussed above are illustrated in Figs 4 and 5. There are two points to note from these probability figures. First, along the track of maximum probability in these figures, the value of the associated bolometric far-IR luminosity of the galaxy changes by only 5–10 per cent. This is much less variation than the factor of 2 variation across the wider range of the  $T$ – $\beta$  parameter space shown in Fig. 2. Secondly,  $F_{\text{wc}}$  is not defined accurately even by the excellent data for NGC 958, as shown in Fig. 5. Hence, this is likely to provide the least

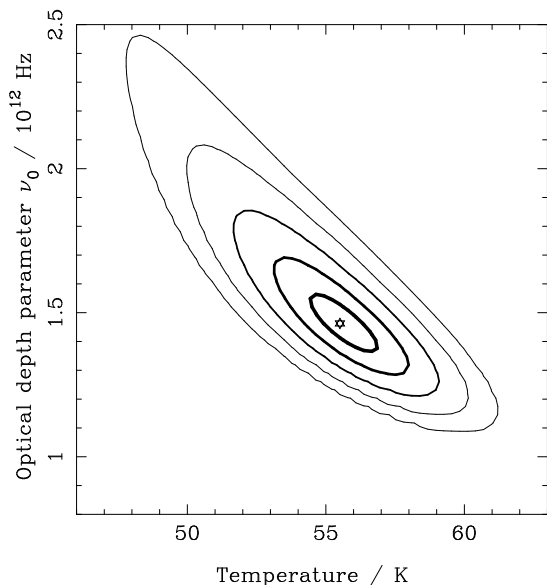


**Figure 4.** The counterpart to Fig. 2, for the optically thick SED (model 2) fitted to data for Arp 220. The shape of the probability contours illustrates the degeneracy between temperature and the frequency at which a galaxy becomes optically thick,  $\nu_0$ .  $\alpha = 3.0$  and  $\beta = 1.5$  are assumed, the best-fitting values.

informative presentation of SED data amongst the four models used. For APM 08279+5255, the extra population of 20-K dust in this model can be seen generating a break in the low-frequency slope of the SED in Fig. 1. The mass of cold dust present in far-IR luminous galaxies may dominate the total mass of dust at all temperatures, and provide information concerning the history of metal enrichment within, but it is far from energetically dominant, and difficult to measure to better than a factor of a few.

For consistency with our earlier treatments (Blain et al. 1999a, 2002; Barnard & Blain 2003) we will adopt the  $T$ - $\alpha$ - $\beta$  model (model 1) in the following discussions. Subject to the effective dust temperature  $T$  being slightly different from that in the other SED parametrizations, this model provides a good description of observations for galaxies ranging from low-luminosity spirals to the most luminous high-redshift systems (Fig. 1). The results that follow are not only valid for this description of the SED, but are generic results that apply to all 4 descriptions discussed above.

### 3 PHOTOMETRIC REDSHIFTS

The well-defined pseudo-thermal SED of dusty galaxies (Fig. 1) offers a prospect of recognizing the redshifts of galaxies with the same intrinsic SEDs by comparing far-IR and submm colours. This was discussed in the context of identifying high-redshift galaxies amongst more numerous low-redshift galaxies in a shallow submm-wave survey by Blain (1998) and for observations of the first generation of hard-to-identify submm galaxies, with flux-density limits from *IRAS* observations by Hughes et al. (1998) and Eales et al. (1999). Eales et al. noted that it is not possible, a priori, to be certain of whether a dusty galaxy is hot and far away, or cool and close by, and that there could be significant consequences for

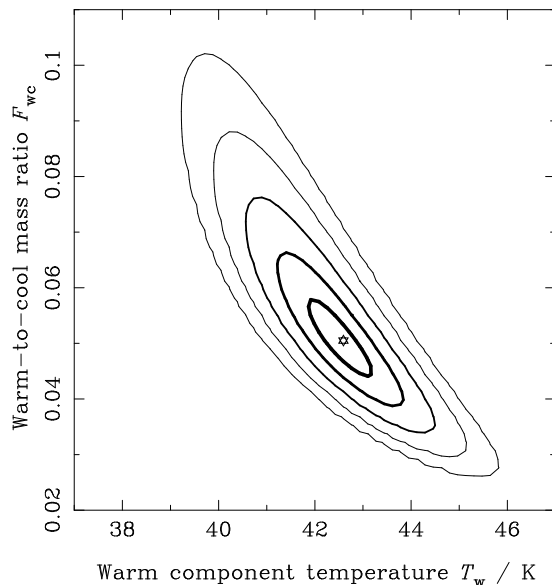


**Figure 5.** An illustration of the significant degeneracy between the warm dust temperature parameter  $T_w$  and the warm dust mass fraction parameter  $F_{wc}$  obtained from fitting to the SED data for Arp 220, at a known redshift  $z = 0.018$  using the two-temperature model 3. The large extent of the error ellipse in the direction of  $F_{wc}$  reflects the general difficulty of determining a dust mass from SED data, illustrating the difficulty of associating parameter values in an SED fit with the true physical properties of dust grains in an observed galaxy.

the cosmological implications of the population of submm-luminous galaxies if the dust temperature/redshift is not estimated correctly. If the dust temperature defining the SED is too hot, and/or the redshift of the population is too great, then the cosmological importance of submm galaxies can be overstated. The reason for the similar effects of increasing both redshift and temperature is that the peak of the SED is determined by the value of  $\nu/T$  in the exponential term of the Planck function. Redshifting the spectrum by a factor of  $(1+z)$  in frequency  $\nu$  thus has a directly equivalent effect to modifying the temperature  $T$  by the same fraction.

By assuming a narrow range of SED templates, with a tight distribution of dust temperatures, when trying to match a redshift (Hughes et al. 2002; Dunlop et al. 2003), this large degeneracy can appear to vanish, leading to unrealistically optimistic estimates of the accuracy of the derived redshifts to  $\Delta z \simeq 0.5$ . Unless a representative range of SED templates is available, perhaps including the full range of observed SEDs of dusty galaxies, with temperatures from less than 20 K (Reach et al. 1995) to more than 80 K (Table 1), then the errors on photometric redshifts could be underestimated. The true error is at least as great as the fractional uncertainty in the dust temperature, even if there are very small errors on the photometric data itself.

This dust temperature-redshift degeneracy is illustrated in Fig. 6 for the photometric data available for both the low-redshift low-luminosity galaxy NGC 958, which includes radio data, and the high-redshift, high-luminosity dusty QSO APM 08279+5255. The availability of radio data reduces the degeneracy somewhat, as the different emission mechanisms lead to different spectral indices (Carilli & Yun

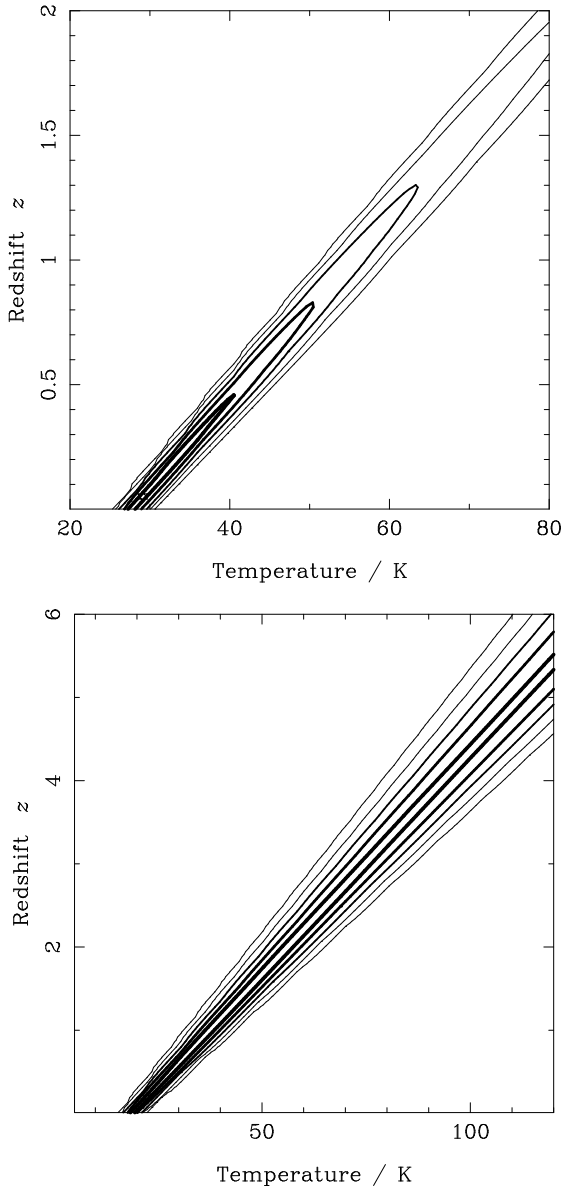


**Figure 6.** An illustration of the degeneracy between the dust temperature  $T$  and the redshift  $z$  fitted to SED data for two dusty galaxies in Fig. 1, disregarding their known redshifts: NGC 958 at  $z = 0.019$  (upper panel) and APM 08279+5255 at  $z = 3.8$  (lower panel). The  $T$ - $\alpha$ - $\beta$  model 1 SED is assumed, with  $\alpha$  and  $\beta$  fixed at their values from Table 1 to minimize the scatter in the fitted values. The data define a narrow track aligned with the locus of constant  $T/(1+z)$ . The radio data for NGC 958 leads to the reduction in probability from low to high temperatures along the track of the contours in the upper panel. Observations of colours alone, even with radio data, provide a strong constraint only on the ratio  $T/(1+z)$ .

1999; Yun & Carilli 2002); however, the radio-submm colour is still a much better indicator of the ratio  $T/(1+z)$  than of  $T$  and  $z$  separately (Blain 1999a). The degeneracy lies along the locus  $T \propto (1+z)$ : see Fig. 6. If a fraction of the radio emission is generated by an AGN, then the derived redshift will be underestimated by perhaps a large amount.

A practical example of a high-redshift galaxy for which

photometric redshifts may be sought is SMM J14011+0252, with a known redshift  $z = 2.56$  (Frayer et al. 1999), and a well determined radio-far-IR SED (Ivison et al. 2001). The galaxy has an achromatic gravitational lensing magnification of a factor of 2.5. Upper limits from *IRAS* provide weak constraints on its dust temperature and mid-IR spectral index  $\alpha$ . Values of  $T$  and  $z$  that provide good fits to the SED data are shown in Fig. 7, setting aside the known redshift  $z = 2.56$ . The true redshift corresponds to  $T \simeq 33$  K; note, however, that the extent of the  $1\sigma$  probability contour in the fit, even in the lower panel for which the assumed fractional errors on the photometric data points are reduced to an artificially low 2 per cent, is  $T = 29_{-9}^{+14}$  K or  $z = 2.2 \pm 1.2$ , hardly useful redshift information. Without increasing the accuracy of the observed data, no useful result for redshift  $z$  alone can be quoted, as the probability contours are open in the upper panel.

### 3.1 A luminosity-temperature ( $LT$ ) relation to the rescue?

The fit for SMM J14011+0252, even with greater observational accuracy assumed, shows the large degeneracy between temperature and redshift when fitting photometric data. Is it possible to improve the redshift accuracy by inferring the luminosity for the galaxy if  $T$  and  $z$  are taken to lie along the tracks of maximum probability in the direction of  $T = (1+z)$  in Figs 5–7? If there is a known link between luminosity and dust temperature, an  $LT$  relation (Dunne et al. 2000; Dale et al. 2001; Blain et al. 2002; Dale & Helou 2002; Barnard & Blain 2003; Chapman et al. 2003), then a colour-magnitude diagram could be used to locate galaxies on the degenerate  $T = (1+z)$  tracks, allowing redshifts to be determined. The inclusion of luminosity information is an implicit assumption in the photometric redshift technique with a narrow range of SED parameters discussed by Hughes et al. (2002), Aretxaga et al. (2003) and Dunlop et al. (2003).

In Fig. 8 we show the bolometric luminosity  $L$  inferred for each temperature  $T$  and redshift  $z$  along the track of maximum probability in both the upper and lower panels of Fig. 7. The luminosity is plotted as a function of temperature, but the unique redshift associated with each temperature can be read from the tracks in Fig. 7. The ranges of fitted  $LT$  values that lie within  $1\sigma$  of the most probable track in Fig. 7 are also shown enclosed by the thinner solid and dashed lines in Fig. 8. The inferred luminosity increases with increasing temperature/redshift, and does so more rapidly than the  $LT$  relation inferred for low-redshift *IRAS* galaxies by Chapman et al. (2003), which is shown by the dotted lines in Fig. 8 and has a scatter of 0.14 dex in the interquartile range.

By comparing the two panels of Fig. 7 and the form of the  $LT$  curves for each panel shown in Fig. 8 it is clear that reducing the size of the errors on the photometric data does not change the width of the inferred track in the luminosity-temperature/redshift space significantly, whereas including luminosity information does restrict the range of plausible temperatures/redshifts for galaxies with photometric data to those lying between the thin dotted lines. Note, however, that the  $1\sigma$  spread in the low-redshift  $LT$  relation covers a range  $T = 38 \pm 10$  K, a dispersion of about 25 per cent.

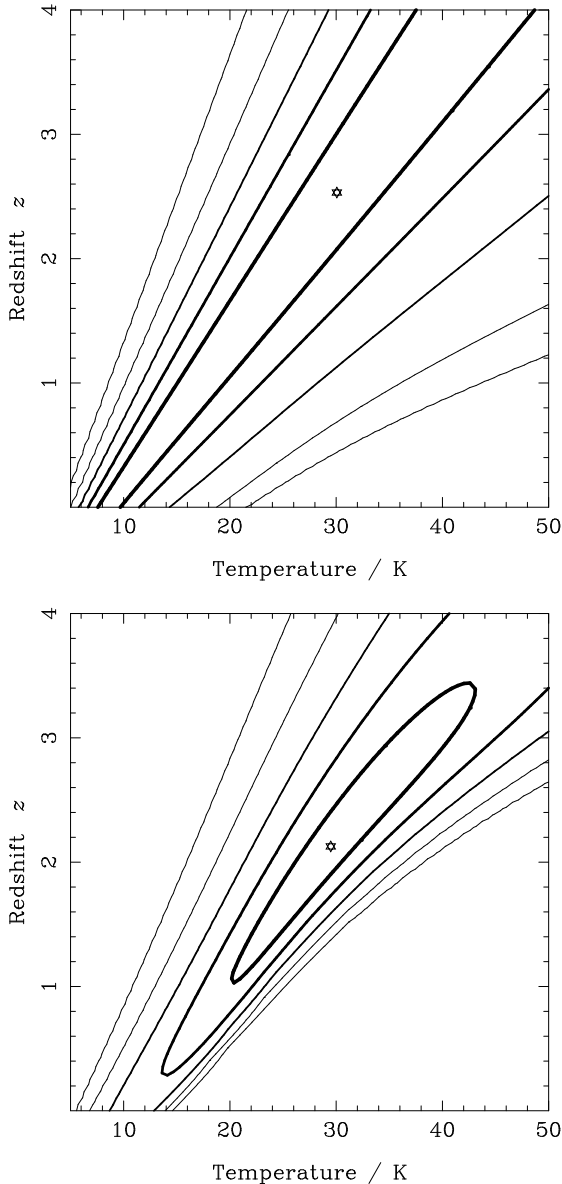


**Figure 7.** A fit to temperature and redshift derived from all existing data for the  $z = 2.56$  submm galaxy SMM J14011+0252 (Frayer et al. 1999; Ivison et al. 2001). In the upper panel the true observational errors are assumed, while in the lower panel the fractional errors are set to only 2 per cent, about five times better than the real data. In both panels there is a huge degeneracy in the direction  $T \propto 1 + z$ , and so little meaningful redshift information is available from the colours alone, even with unrealistically small errors. In the lower panel there is a clear maximum probability. The best-fitting line is also deflected between low and high temperatures due to the different temperature dependence of the submm and radio SEDs.

The associated redshift, obtained by reading off the maximum probability track in Fig. 7, based on unrealistically accurate data, indicates a range  $z = 2.9 \pm 0.9$ : the result for less precise existing data shown in the upper panel of Fig. 7 is  $z = 3.4 \pm 1.1$ . While these ranges include the true redshift  $z = 2.56$ , the uncertainties make the results of little use when compared to the exact values of  $T$  and  $L$  that

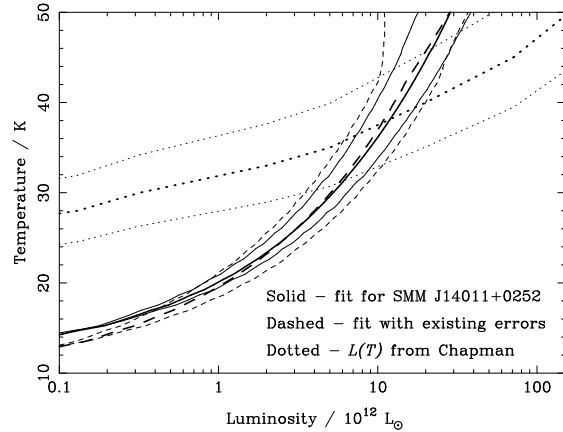


**Figure 8.** The bolometric luminosity inferred from photometric data for SMM J14011+0252, as a function of temperature in the restframe of the galaxy along the permitted track of maximum probability in the  $T$ - $z$  parameter space as shown in Fig. 7. The results derived assuming both existing errors (dashed lines) and tighter 2 per cent errors (solid lines), are similar. The thin lines enclosing the thick lines trace out the region of the figure occupied by  $LT$  values within one standard deviation of the best-fit track through each part of Fig. 7. In both cases the luminosity is corrected for the known magnification factor of 2.5. Each temperature corresponds to a different redshift  $T \propto (1 + z)$ . At the known redshift  $z = 2.56$  the fitted temperature is approximately 35 K (Fig. 6). The low-redshift  $LT$  relation derived from *IRAS* data and its 0.14-dex interquartile range uncertainty (Dale et al. 2001; Dale & Helou 2002; Chapman et al. 2003) is shown by the thick and thin dotted lines respectively. The uncertainty in the  $LT$  relation dominates the error on an inferred  $T$ - $z$  value. The scatter in temperature  $T$  by approximately 15 per cent corresponds to a scatter in inferred  $z$  by approximately 25 per cent.

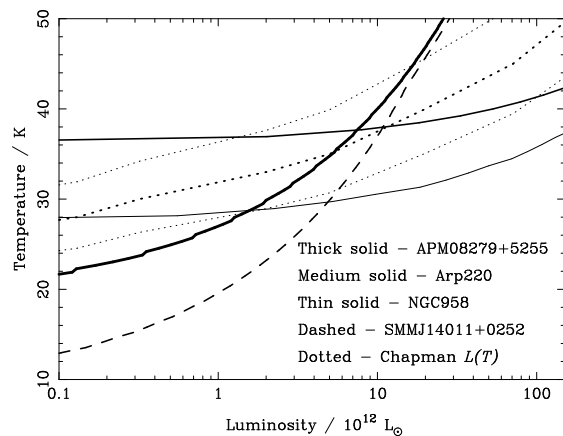


**Figure 9.** The bolometric luminosity inferred from photometric data for the  $z = 0.019$  spiral galaxy NGC 958, the  $z = 0.018$  ULIRG Arp220 and the ultraluminous  $z = 3.87$  galaxy APM 08279+5255 (demagnified by a factor of 50), compared with the result for SMM J14011+0252 and the low-redshift  $LT$  relation shown in Fig. 8. The errors on the track traced for all three galaxies are very small. The curves for NGC 958 and Arp220 intersect the  $LT$  relation close to their expected temperatures, but the curve for APM 08279+5255 does not.



could be found from a spectroscopic redshift. The spread in the derived redshifts, assuming the measured scatter in the low-redshift  $LT$  relation (Chapman et al. 2003) is a factor of 2 greater than the photometric redshift accuracy claimed from the SMM J14011+0252 data by Hughes et al. (2002;  $z = 2.9^{+0.6}_{-0.4}$ ). The corresponding range in luminosity covers  $6 \times 10^{12}$  to  $2 \times 10^{13} L_{\odot}$ , a factor of approximately 3 (Fig. 8). Photometric redshifts cannot be obtained to the accuracy proposed by Hughes et al. (2002) without assuming an unreasonably tight dispersion in the  $LT$  relation, by taking an inadequate range of SED functions into account.

Knowledge of an  $LT$  relation for submm galaxies is thus unlikely to rescue far-IR/submm/radio photometric redshifts from the temperature-redshift degeneracy. The error in the derived temperature/redshift for an individual galaxy is expected to be dominated by the uncertainty in the  $LT$  relation. Once a spectroscopic redshift is obtained for a submm galaxy, however, its temperature and luminosity can be determined quite accurately: compare the widths of the probability contours in Figs 5–7 at constant redshift. Temperatures and luminosities accurate to about 20 and 50 per cent, respectively, are thus expected.

Note that the Chapman et al. (2003) low-redshift  $LT$  relation shown by the dotted lines in Fig. 8 is consistent with estimates of the temperature of the bulk of the submm-selected galaxy population derived by comparing their multiwavelength properties (Blain et al. 1999; Trentham, Blain & Goldader 1999). Using the  $T$ - $\alpha$ - $\beta$  SED description (equation 1), these temperatures lie close to 40 K at luminosities of several  $10^{12} L_{\odot}$ , assuming a high redshift ( $z > 1$ ).

The SEDs discussed earlier, for NGC 958, Arp 220 and APM 08279+5255, can be analyzed in the same way as the data for SMM J14011+0252 shown in Fig. 8.<sup>2</sup> The resulting tracks in the  $LT$  diagram are shown in Fig. 9. The  $LT$  curves for NGC 958 and Arp 220 intersect with the low-redshift Chapman et al.  $LT$  relation at temperatures of approximately 28 and 38 K respectively. These results are very close to their fitted temperatures, taking into account their redshifts, which are 29 and 38 K respectively in model 1 (Table 1). Hence, in the absence of redshift information, a photometric redshift derived for both of these galaxies would be reliable, although the uncertainty would be dominated by the  $LT$  relation.

However, the curves intersect for APM 08279+5255 at  $T \simeq 34$  K, nowhere near its true temperature  $T \simeq 80$  K (in model 1), even after correcting for magnification by an assumed factor of 50. This is at least a warning that some galaxies would have a very discrepant photometric redshifts derived from far-IR and submm data using this technique. This galaxy is significantly hotter than other high-redshift dusty galaxies, but it is certainly an interesting object, and owing to its great luminosity, one that could be found quite easily in future far-IR and submm-wave surveys. The observational errors for all three of these brighter galaxies are

<sup>2</sup> SMM J14011+0252 seems to set an unfortunate precedent for studies of submm galaxies: it is unusually bright in the optical range, and it shows no sign of the presence of an AGN, unlike most other identified galaxies (Smail et al. 2002). It lies squarely on the radio-far-IR correlation. Although it is relatively easy to study, SMM J14011+0252 is perhaps unrepresentative of submm galaxies as a whole.

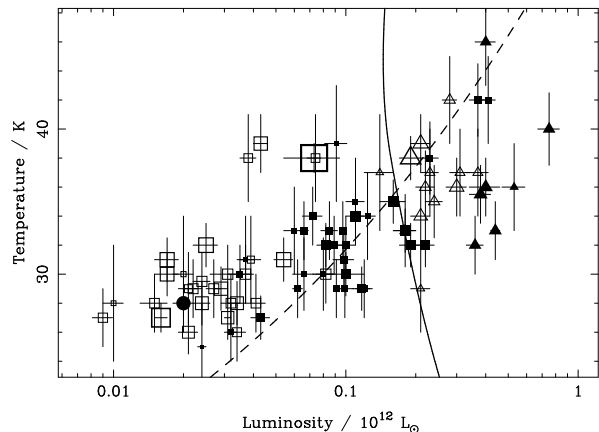


**Figure 10.** The  $LT$  values derived for 83 *IRAS* BGS galaxies observed by SCUBA (Dunne et al. 2000), fitted using the  $T$ - $\alpha$ - $\beta$  SED description. The different symbols represent different redshifts:  $z < 0.01$ , open square;  $0.01 \leq z < 0.02$ , filled square;  $0.02 \leq z < 0.03$ , empty triangle;  $0.03 \leq z < 0.04$ , filled triangle;  $0.04 \leq z < 0.05$ , empty circle; and  $z \geq 0.05$ , filled circle. Larger symbols represent more accurate results. The overplotted solid and dashed lines trace the loci of a 0.5-Jy 60- $\mu$ m source and a 60-mJy 850- $\mu$ m source, respectively, both at  $z = 0.02$ . They show the direction in which observational selection effects could truncate the distribution of points. The dashed 850- $\mu$ m curve runs parallel to the distribution of the data points, and so there might be a selection effect against detecting hot sources in the sample. However, almost all the targeted *IRAS* sources were detected at 850  $\mu$ m, and so the lack of sources at the top left of the field probably reflects a genuine absence of hot, low-luminosity galaxies in the *IRAS* sample.

much smaller than for SMM J14011+0252, and so the discrepancies in their photometric redshifts definitely reflect a dispersion in the  $LT$  relation rather than errors in the data points.

In order to estimate reliable photometric redshifts from submm, far/mid-IR and radio observations it is necessary to be certain of the nature of and scatter in the  $LT$  relation. This can be investigated using a variety of samples of IR-luminous galaxies with known redshifts. It is also important to determine whether the relation evolves with redshift. If it does, then this could provide insight into the astrophysics of dusty galaxies, in addition to important information for finding photometric redshifts.

### 3.2 Observed $LT$ relations

The accurate determination of the temperature and luminosity of dusty galaxies with known redshifts using a three-parameter  $T$ - $\alpha$ - $\beta$  SED description was illustrated above. In order to determine a temperature reliably, the redshift must be known, and flux density data must be available at frequencies both above and below the peak of the SED. Radio data can be used as a proxy for mid-/far-IR data if the galaxies can be assumed to lie on the far-IR-radio correlation. The number of galaxies for which all the required far-IR/radio and submm information is available is relatively small. We now derive  $LT$  relations from three different sam-

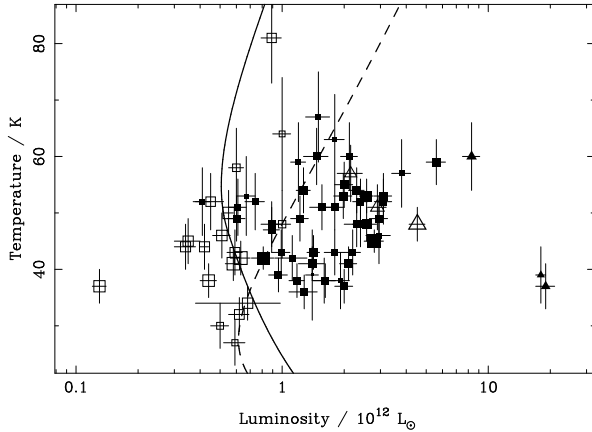


**Figure 11.** The  $LT$  relation of 72 galaxies in both the *IRAS* Faint Source Catalog and the VLA-FIRST radio survey catalogue (Stanford et al. 2000), fitted using the  $T$ - $\alpha$ - $\beta$  SED description. The different symbols represent different redshifts:  $z < 0.1$ , open square;  $0.1 \leq z < 0.2$ , filled square;  $0.2 \leq z < 0.3$ , empty triangle;  $0.3 \leq z < 0.4$ , filled triangle;  $0.4 \leq z < 0.5$ , empty circle; and  $z \geq 0.5$ , filled circle. Better fitting data are plotted using a larger symbol. The solid and dashed overplotted lines show the direction in which observational selection effects would be important, and trace the loci of a 100-mJy 60- $\mu$ m source and a 1-mJy 1.4-GHz source, respectively, both at  $z = 0.25$ . Both curves cut directly across the cloud of points, and so the lack of sources away from the cloud of points at luminosities  $L > 10^{12} L_{\odot}$  is not likely to be due to selection effects.

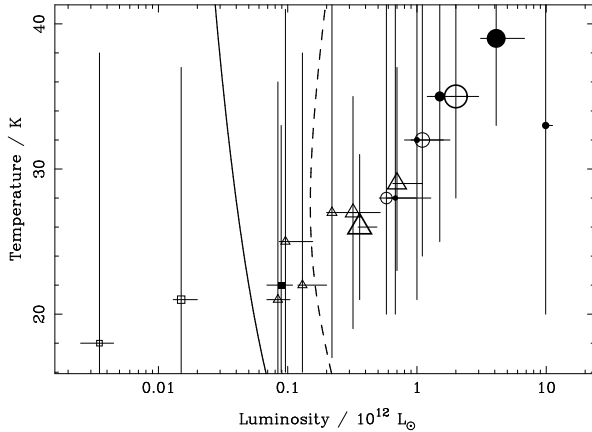


**Figure 12.** The  $LT$  relation for 18 galaxies detected at radio wavelengths using MERLIN and in the mid-IR using *ISO* in the HDF (Garrett 2002), fitted using the  $T$ - $\alpha$ - $\beta$  SED description (equation 1). The different symbols represent different redshifts:  $z < 0.2$ , open square;  $0.2 \leq z < 0.4$ , filled square;  $0.4 \leq z < 0.6$ , empty triangle;  $0.6 \leq z < 0.8$ , filled triangle;  $0.8 \leq z < 1$ , empty circle; and  $z \geq 1$ , filled circle. Larger symbols represent more accurate results. Note that the temperatures are derived by assuming that the far-IR–radio correlation holds, and their errors are much larger than those for the other samples shown in Figs 10 and 11. The solid and dashed overplotted lines show the direction in which observational selection effects would be important, and trace the loci of a 0.5-mJy 15- $\mu$ m source and a 50- $\mu$ m 1.4-GHz source respectively, both at  $z = 0.5$ . Both lines cut directly across the points, and so the lack of sources away from the trend is not likely to arise from selection effects.

ples of galaxies to investigate its properties from the limited existing data.

### 3.2.1 Low-redshift *IRAS* galaxies

We have already discussed the low-redshift  $LT$  relation derived from a large sample of *IRAS* galaxies by Chapman et al. (2003): see the dotted lines in Figs 8 and 9. However, these results are based on radio and far-IR data alone. It would be very useful to include submm data at intermediate wavelengths in order to be sure of the form of the SED.

A much smaller number of low-redshift galaxies in the *IRAS* catalogue were observed at submm wavelengths in the SLUGS survey by Dunne et al. (2000) and Dunne & Eales (2001). The results provide important information about both the local, low-luminosity  $LT$  relation and galaxy SEDs. Many of these galaxies also have radio data from the NED database, and we have exploited this information, assuming the far-IR–radio correlation to improve the accuracy of the derived values of bolometric luminosity and temperature for these galaxies as compared with the SLUGS values. The resulting SEDs are thus obtained by combining radio data with the flux densities at 850, 100 and 60  $\mu$ m considered by Dunne et al. (2000). The resulting quantities for 83 galaxies in the SLUGS sample are shown in Fig. 10, along with two lines that trace the luminosity and temperature of a galaxy that is required to generate the typical flux density of a galaxy in the sample at a typical redshift for the sample. These curves provide an indication of the possible role of selection effects in limiting the extent of the scatter in the derived  $LT$  relation. If the lines lie parallel to a correlation in the plotted points, then some of the correlation could be due to selection effects acting to reduce the intrinsic scatter, by removing galaxies from the sample on the low-luminosity side of the line. This is not the only way in which selection effects could modify the observed or inferred scatter in an  $LT$  relation; however, it provides a direct indication of whether or not selection effects are likely to be significant.

For the SLUGS data, the role of selection effects is unlikely to be very significant, as almost all of the targeted *IRAS* galaxies were detected at submm wavelengths (Dunne et al. 2000). Note that the luminosities and temperatures of the Milky Way (Reach et al. 1995;  $L \sim 3 \times 10^{10} L_{\odot}$ ;  $T \simeq 17$  K) and NGC 891 (Alton et al. 1998;  $L \simeq 5.3 \times 10^9 L_{\odot}$ ;  $T \simeq 20 \pm 2$  K) lie at luminosities slightly below the cloud of data points, whereas the low-luminosity, hot starburst galaxy M82 ( $L \simeq 2.7 \times 10^{10} L_{\odot}$ ;  $T = 42 \pm 2$  K) is significantly offset above the cloud. The apparent dispersion in the  $LT$  relation shown in Fig. 10 may thus be less than the true dispersion. The scatter in the temperatures derived for SLUGS galaxies is comparable to the scatter determined from the SEDs of low-redshift *IRAS* galaxies shown in Fig. 8 (Chapman et al. 2003).

### 3.2.2 VLA–*IRAS* galaxies at moderate redshifts

At higher redshifts, *IRAS* flux densities are available only for the most luminous galaxies. The fluxes from the *IRAS* Faint Source Catalog (FSC) were correlated with data from the wide-field VLA-FIRST radio survey (Becker, White & Helfand 1995) to provide information on the  $LT$  relation for a

large sample of galaxies with bolometric luminosities greater than  $\sim 10^{12} L_{\odot}$  by Stanford et al. (2000). The  $LT$  values for these galaxies were calculated assuming that the far-IR–radio correlation holds. The  $LT$  values for the 72 galaxies from this sample with reliable redshifts, which are not fitted by extremely cold temperatures ( $T < 5$  K) and thus radio-loud, are plotted in Fig. 11. About 25 further galaxies from the sample of Stanford et al. fall into the very cold category, thus indicating a likely  $\sim 25$  per cent contamination fraction in the sample from radio-loud AGN that emit a radio flux density greater than that expected from the observed low-redshift far-IR–radio correlation. The tracks of the lines through the data confirm that neither radio nor IR selection effects should severely bias the  $LT$  relation from the sample of Stanford et al., which lies on a slightly hotter track, and is scattered by a greater amount to higher temperature as compared with the SLUGS sample. This suggests that hotter, perhaps more AGN-rich galaxies, are represented in this more luminous, partially radio-selected sample. A similar sample of about 40 luminous southern galaxies, with radio images from the Molonglo telescope and redshifts from the 2dF multi-object spectrograph has recently been compiled by Sadler et al. (2002), and could be analyzed in a similar way. Our understanding of the  $LT$  relation would be much improved if submm fluxes could be determined for these galaxies with known moderate redshifts and radio and far-IR flux densities. These observations would both provide tighter constraints on their positions in the  $LT$  plane, and offer the possibility to search for evolution in the  $LT$  relation (Chapman et al. 2003).

### 3.2.3 Faint radio and mid-IR selected galaxies in the Hubble Deep Field

Another sample useful for investigating the  $LT$  relation is the 18  $z \sim 1$  faint radio galaxies detected at  $15 \mu\text{m}$  using *ISO* in the Hubble Deep Field (HDF; Garrett 2002). These galaxies are sampled at mid-IR wavelengths much shorter than the peak of their SEDs, but the radio data provides a proxy for the 60–100- $\mu\text{m}$  emission close to the peak, assuming that the far-IR–radio correlation holds. A coarse upper limit to the 60- $\mu\text{m}$  flux densities of the galaxies is provided by an XSCANPI analysis<sup>3</sup> of the relevant *IRAS* scans. A constraint on the 60- $\mu\text{m}$  flux densities of these galaxies is essential for fitting temperatures to the radio–mid-IR data. The inferred  $LT$  relation is shown in Fig. 12: it exhibits a remarkably narrow dispersion, but the errors on the data points are large. Galaxies at the mid-IR wavelengths probed have spectral features associated with emission from PAH molecules, and so this tight correlation is all the more surprising. A link between the intensity of PAH emission and the bolometric luminosity of a galaxy has been commented on for a sample of only five galaxies by Haas, Klass & Bianchi (2002). An apparent link between  $15 \mu\text{m}$  emission and bolometric luminosity for a larger sample of low-redshift galaxies is discussed in Sections 5.3 and 5.5 of Dale & Helou (2002). The tracks of typical galaxies in the sample overplotted on Fig. 11 show that selection effects are unlikely to be responsible for the tight correlation.

It seems unlikely that the mid-IR flux density of a galaxy could be better correlated with its temperature and luminosity than data obtained closer to the peak of the SED. This would require some underlying correlation between the slope of the mid-IR SED and the total luminosity that is not apparent in existing datasets. Much larger samples from *SIRTF* from 2003 will hopefully resolve this question.

### 3.2.4 Submm-selected high-redshift galaxies

A few distant submm- and far-IR-selected galaxies (Ivison et al. 1998, 2000, 2001; Frayer et al. 1998, 1999; Chapman et al. 2002a) also have redshifts, and many more have recently been found using deep radio-selected galaxies (Chapman et al. 2002b). Initial results indicate that it is likely that the values of temperature and luminosity derived for high-redshift submm-selected dusty galaxies display a similar scatter to that shown in Fig. 11. These samples are destined to grow in size, and will provide the ultimate test of the high-redshift  $LT$  relation and the reliability of far-IR photometric redshifts for high-redshift galaxies. This sample is extremely useful, as it consists of the target population for which photometric redshifts are sought at far-IR and submm wavelengths. Inferred values of luminosity and temperature for high-redshift dusty galaxies with known redshifts can be found in Chapman et al. (2002b).

## 3.3 $LT$ relations from a combination of samples

The combined  $LT$  relation for all three samples is compared in Fig. 13, segregated between samples by the plotting symbol. The  $LT$  relations estimated for low-redshift *IRAS* galaxies by Chapman et al. (2003), based on 60–100  $\mu\text{m}$  colours and the SED templates of Dale et al. (2001), and for both merging and quiescent galaxies at low redshifts by Barnard & Blain (2003) are represented by the lines. Note that the temperature inferred by Chapman et al. (2003) is  $T_{\text{min}}$  as defined in equation (4), and so is lower by 10–20 per cent as compared with the definitions used here, reducing the difference between the solid line that represents the Chapman et al.  $LT$  relation and the dashed line representing the  $LT$  relation for luminous merging galaxies.

The dispersion in the  $LT$  relation exceeds 25 per cent (0.1 dek) at all luminosities. These results demonstrate that the dispersion in the  $LT$  relation within individual samples is less than the dispersion between samples. The Stanford et al. sample is more likely to be significantly affected by radio emission from AGN, which could introduce additional scatter, causing an overestimate of luminosity and an underestimate of temperature. High-luminosity sources that would be selected in submm-wave surveys are thus observed to have dust temperatures that range between 25 and 60 K. The median temperature and its RMS scatter in temperature are about  $45 \pm 10$  K, a dispersion of approximately 0.1 dek.

Galaxies with low dust temperatures are difficult to select in the far-IR surveys from which these  $LT$  results are drawn, and so there may not necessarily be a lack of very luminous cool galaxies, despite the avoidance of points at the lower right corner of Fig. 13. By contrast, there appears to be a real lack of hot, low-luminosity galaxies from the SLUGS and Stanford et al. *IRAS*-selected galaxies. An exception is one of the closest, brightest *IRAS* galaxies, M82.

<sup>3</sup> <http://www.ipac.caltech.edu/ipac/services/xscanpi.html>

Despite its low luminosity of only  $2.7 \times 10^{10} L_{\odot}$ , M82 has a temperature of  $42 \pm 2$  K, in the empty upper left region of the figure. Such hot, dwarf galaxies are difficult to find in the *IRAS* survey, on the grounds of the limited survey volume for low-luminosity galaxies; however, much deeper surveys using *SIRTF* may find that this region of the *LT* plane is more thoroughly populated with moderate-redshift galaxies.

The same points are replotted in Fig. 14, segregated by the plotted symbol in redshift rather than from sample to sample. There is a natural tendency for more luminous galaxies to be selected at greater redshifts. As the population of dusty galaxies is known to evolve strongly in luminosity with redshift, this trend should be all the more apparent. However, at all redshifts the scatter in the *LT* relation from sample to sample appears to span the full range of the scatter seen in the combined population. The dispersion thus appears to reflect a real spread in the physical properties of galaxies present at all redshifts, and not to be due solely to a systematic evolution in a tightly dispersed *LT* relation with redshift. There is no strong evidence in samples of *IRAS*-selected galaxies for the *LT* relation to evolve with redshift over the approximate range  $0 < z < 0.3$  (Chapman et al. 2003).

The significant dispersion in the *LT* relation indicates that there are limited opportunities for discriminating between hot–distant and cool–closer galaxies on the grounds of their far-IR/submm colours even with an assumed *LT* relation. With an *LT* dispersion of at least 25 per cent (Fig. 13), the fractional accuracy of a photometric redshift determination is never likely to be better than 30 per cent. Current evidence thus suggests that spectroscopic redshifts will remain essential to interpret the nature of submm-selected galaxies, unless increased sample sizes reveal that the existing samples of high-redshift dusty galaxies are scattered by a larger amount in the *LT* plane than the true distribution, which is currently well determined only at low redshifts (Chapman et al. 2003). We think that this is unlikely, and rather that the observed scatter in the distribution will remain the same or grow larger as more information becomes available. Larger samples will provide a better description of the distribution of galaxies in the wings of the *LT* distribution, and unearth further examples of rare galaxies like M82 and APM 08279+5255, that are not represented in the *LT* plane at the current sampling rate.

#### 4 FUTURE SED MEASUREMENTS

The greatest change in our understanding of the properties of dusty galaxies will be brought with the launch of *SIRTF* in 2003 January. With a 0.85-m aperture, and capable of diffraction-limited imaging in far-IR bands at effective wavelengths of 24, 70 and  $160 \mu\text{m}$ , *SIRTF* will provide key information on the SEDs of at least several million galaxies. Unlike galaxies detected by *IRAS*, these will extend well beyond a redshift of 1, and will be located to an accuracy of order 5 arcsec. By combining the positions of galaxies detected by *SIRTF* with spectroscopic redshifts obtained as part of the Sloan Digital Sky Survey (SDSS), which is reasonably complete to  $z \simeq 0.3$ , it should be possible to obtain SED data for of order  $10^4$  galaxies with exact redshifts, and

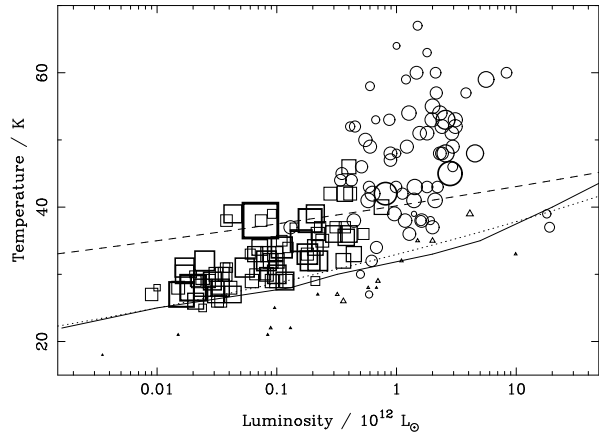


**Figure 13.** The combined *LT* scatter for all galaxies shown in Figs 9–11: Dunne et al. (2000), squares; Garrett (2002), lozenges; and Stanford et al. (2000), circles. The better-fitting galaxies are represented by larger symbols. The overplotted lines show the results from other low-redshift *LT* investigations: the solid line shows the result of Chapman et al. (2003), and the dashed and dotted lines represent the results for merging and quiescent galaxies by Barnard & Blain (2003) respectively. Galaxies appear to avoid the hot, low-luminosity region to the upper left of the figure, which is not likely to be empty due to systematic selection effects.

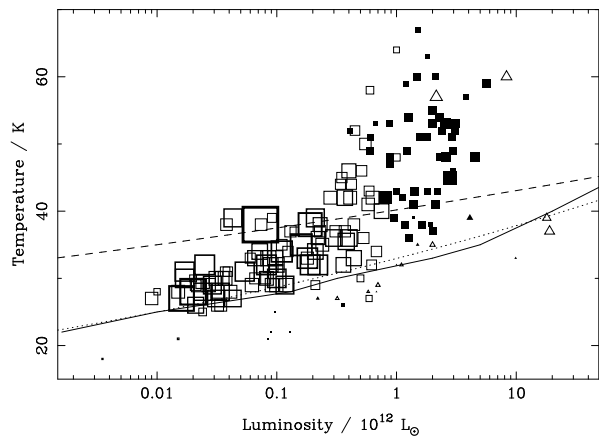


**Figure 14.** The combined *LT* relation illustrated in Fig. 12, this time as a function of redshift. Galaxies at  $z \leq 0.2$  are represented by empty squares, at  $0.2 < z \leq 0.5$  by filled squares, at  $0.5 < z \leq 1$  by empty triangles, at  $1 < z \leq 2$  by filled triangles, at  $2 < z \leq 3$  by empty circles and at  $z > 3$  by filled circles. There is a natural trend to greater luminosities/temperatures at higher redshifts. In each redshift interval temperatures range over the full extent of the scatter in the diagram, and there is no evidence for a significant change in the *LT* relation with redshift (Chapman et al. 2003).

thus to determine the form of the *LT* relation discussed in Fig. 14 in much more detail. At that point the accuracy of photometric redshifts based on far-IR colours combined with an *LT* relation can be assessed realistically, at least at low to moderate redshifts.

The information can be extended out to higher redshifts by considering optical photometric redshifts, derived

reliably from spectral breaks in the SDSS data for galaxies too faint/distant to be targeted for SDSS spectroscopy. At the same time, many of the galaxies with known high redshifts shown in Fig. 14, which already have some spectral information at far-IR/submm wavelengths, will be targets for *SIRTF*. More information will thus soon be available about their SEDs. By combining radio observations with several far-IR data points it should be possible to generate a more accurate *LT* relation, and to measure any changes in the far-IR–radio correlation with increasing redshift by the end of *SIRTF*'s mission in approximately 2008. The true potential for far-IR and submm-wave photometric redshifts can then be assessed securely. The reliability of the far-IR–radio correlation can in the meantime be investigated using data for any galaxy with a known redshift that has three accurate flux density measurements, one each at radio, submm and far-IR wavelengths.

## 5 CONCLUSIONS

We have discussed the description of the SEDs of dusty galaxies using four different models that are appropriate to describe data that is available at present and is likely to be generated by forthcoming space missions. One of the parameters in each model always describes the peak frequency of the thermal dust SED ('temperature'), while two spectral indices describe the fraction of hot and cold dust: an ' $\alpha$ ' and ' $\beta$ ' parameter respectively. Observational data constrains these SED descriptions to within 10 per cent accuracy across the full range of interesting wavelengths longer from about  $20\ \mu\text{m}$  to deep in the radio waveband. It is important to be careful in interpreting the values of dust temperatures, emissivities and masses that are inferred with the values of real physical parameters.

There is a huge degeneracy between temperature and redshift when fitting the SED of a distant galaxy. Assuming some link between the luminosity and SED allows this degeneracy to be broken, but a range of available information indicates that this relationship has a very considerable scatter, by up to a factor of 2. Without the knowledge that this *LT* relation has a scatter as narrow as the required accuracy of the photometric redshift, continuum far-IR/submm/radio photometric redshifts are almost useless for providing constraints from the data for an individual galaxy.

In order to finally assess their usefulness it is essential to quantify the *LT* relationship accurately, based on a large number of galaxies with known redshifts and well-sampled SEDs. This information is not available at present, but will be generated by *SIRTF*. Only if the true scatter in the *LT* relation turns out to be less than about 20 per cent will the photometric redshift technique be useful. Spectroscopic observations to fix the redshifts and SEDs of dusty galaxies remain essential to understand the population, and it is important to develop new types of spectroscopic instruments that can address these questions, for example wide-band detectors for multiple CO emission lines (Bradford et al. in preparation).

## ACKNOWLEDGMENTS

This research has made use of the NASA/IPAC Extragalactic Database (NED) which is operated by the Jet Propulsion Laboratory, California Institute of Technology, under contract with the National Aeronautics and Space Administration. We thank the referee Danny Dale for a very rapid and helpful report.

## REFERENCES

- Alton P. B., Bianchi S., Rand R. J., Xilouris E. M., Davies J. I., Trewhealla M., 1998, *ApJ*, 507, L125
- Aretxaga I., Hughes D. H., Chapin E. L., Gaztanaga E., Dunlop J. S., 2002, *MNRAS*, submitted (astro-ph/0205313)
- Barnard V. E., Blain A. W., 2003, *MNRAS*, submitted
- Becker R. H., White R. L., Helfand D. J., 1995, *ApJ*, 450, 559
- Benford D. J., Cox P., Omont A., Phillips T. G., 1999, *ApJ*, 518, L65
- Blain A. W., 1998, *MNRAS*, 297, 511
- Blain A. W., 1999a, *MNRAS*, 304, 669
- Blain A. W., 1999b, in R. J. Weymann et al. eds. *Photometric Redshifts and High Redshift Galaxies*, ASP Conf. Series Vol. 191, Astron. Soc. Pac, San Francisco, p. 255 (astro-ph/9906141)
- Blain A. W., Smail I., Ivison R. J., Kneib J.-P., 1999, *MNRAS*, 302, 632
- Blain A. W., Frayer D. T., Bock J. J., Scoville N. Z., 2000, *MNRAS*, 313, 559
- Blain A. W., Smail I., Ivison R. J., Kneib J.-P., Frayer D. T., 2002, *Physics Reports*, 369, 111 (astro-ph/0202228)
- Bradford C. M. et al., in preparation
- Carilli C. L. et al., 2001, *ApJ*, 555, 625
- Carilli C. L., Yun M. S., 1999, *ApJ*, 513, L13
- Chapman S. C., Smail I., Ivison R. J., Helou G., Dale D. A., Lagache G., 2002a, *ApJ*, 573, 66
- Chapman S. C., Blain A. W., Ivison R. J., Smail I., 2002b, *Nature*, submitted
- Chapman S. C., Helou G., Lewis G. F., Dale D. A., 2003, *ApJ*, in press
- Combes F., Maoli R., Omont A., 1999, *A&A*, 345, 369
- Condon J. J., 1992, *ARA&A*, 30, 575
- Dale D. A., Helou G., Contursi A., Silbermann N. A., Khatkar S., 2001, *ApJ*, 549, 215
- Dale D. A., Helou G., 2002, *ApJ*, 576, 159
- Devriendt J., E. G., Guiderdoni B., Sadat R., 1999, *A&A*, 350, 381
- Dunlop J. S. et al., 2002, *MNRAS*, submitted (astro-ph/0206432)
- Dunne L., Eales S., Edmunds M., Ivison R., Alexander P., Clements D. L., 2000, *MNRAS*, 315, 115
- Dunne L., Eales S. A., 2001, *MNRAS*, 327, 697
- Eales S. A., Lilly S., Gear W., Dunne L., Bond J. R., Hammer F., Le Fèvre O., Crampton D., 1999, *ApJ*, 515, 518
- Efstathiou A., Rowan-Robinson M., Siebenmorgen R., 2000, *MNRAS*, 313, 734
- Frayer D. T., Ivison R. J., Scoville N. Z., Yun M. S., Evans A. S., Smail I., Blain A. W., Kneib J.-P., 1998, *ApJ*, 506, L7
- Frayer D. T. et al., 1999, *ApJ*, 514, L13
- Garrett M., 2002, *A&A*, 384, L19
- Granato G. L., Danese L., Franceschini A., 1996, *ApJ*, 460, L11
- Haas M., Klaas U., Bianchi S., 2002, *A&A*, 385, L23
- Hildebrand R. H., 1983, *QJRAS*, 24, 267
- Hughes D. H. et al., 1998, *Nature*, 394, 241
- Hughes D. H. et al., 2002, *MNRAS*, 335, 871
- Irwin M. J., Ivison R. A., Lewis G. F., Totten E. J., 1998, *ApJ*, 505, 529
- Isaak K. G. et al. 2002, *MNRAS*, 329, 149

- Iverson R. J., Smail I., Le Borgne J.-F., Blain A. W., Kneib J.-P., Bézecourt J., Kerr T. H., Davies J. K., 1998, MNRAS, 298, 583
- Iverson R. J., Smail I., Barger A. J., Kneib J.-P., Blain A. W., Owen F. N., Kerr T. H., Cowie L. L., 2000, MNRAS, 315, 209
- Iverson R. J., Smail I., Frayer D. T., Kneib J.-P., Blain A. W., 2001, ApJ, 561, L45
- Lewis G. F., Chapman S. C., Ibata R. A., Irwin M. J., Totten E. J., 1998, ApJ, 505, L1
- Luhman M. et al., 1998, ApJ, 504, L11
- Malhotra S., 1997, ApJ, 491, L27
- Mazzarella J. M., Balzano V. A., 1986, ApJS, 62, 751
- Popescu C. C., Tuffs R. J., Völk H. J., Pierini D., Madore B. F., 2002, ApJ, 567, 221
- Reach W. T. et al., 1995, ApJ, 451, 188
- Sadler E. et al., 2002, MNRAS, 329, 227
- Sanders D. B. and Mirabel I. F., 1996, ARA&A, 34, 749
- Soifer B., Neugebauer G., 1991, AJ, 101, 354
- Smail I., Iverson R. J., Blain A. W., Kneib J.-P., 2002, MNRAS, 331, 495
- Stanford S. A., Stern D., van Breughel W., De Breuk C., 2000, ApJS, 131, 185
- Trentham N., Blain A. W., Goldader J., 1999, MNRAS, 305, 61
- Yun M. S., Carilli C. L., 2002, ApJ, 568, 88